12-21-2021

Progressive Destabilization and Triggering Mechanism Analysis Using Multiple Data for Chamoli Rockslide of 7 February 2021

Wenfei Mao

Lixin Wu

Ramesh P. Singh

Yuan Qi

Busheng Xie

See next page for additional authors

Progressive Destabilization and Triggering Mechanism Analysis Using Multiple Data for Chamoli Rockslide of 7 February 2021

Authors

Wenfei Mao, Lixin Wu, Ramesh P. Singh, Yuan Qi, Busheng Xie, Yingjia Liu, Yifan Ding, Zilong Zhou, and Jia Li

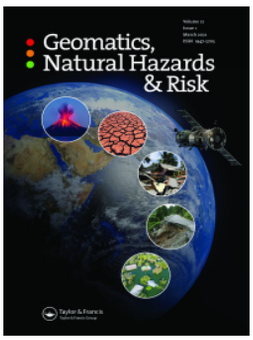

Geomatics, Natural Hazards and Risk

ISSN: (Print) (Online) Journal homepage: https://www.tandfonline.com/loi/tgnh20

Progressive destabilization and triggering mechanism analysis using multiple data for Chamoli rockslide of 7 February 2021

Wenfei Mao, Lixin Wu, Ramesh P. Singh, Yuan Qi, Busheng Xie, Yingjia Liu, Yifan Ding, Zilong Zhou & Jia Li

To cite this article: Wenfei Mao, Lixin Wu, Ramesh P. Singh, Yuan Qi, Busheng Xie, Yingjia Liu, Yifan Ding, Zilong Zhou & Jia Li (2022) Progressive destabilization and triggering mechanism analysis using multiple data for Chamoli rockslide of 7 February 2021, Geomatics, Natural Hazards and Risk, 13:1, 35-53, DOI: 10.1080/19475705.2021.2013960

To link to this article: https://doi.org/10.1080/19475705.2021.2013960

Published online: 21 Dec 2021.

GEOMATICS, NATURAL HAZARDS AND RISK
2022, VOL. 13, NO. 1, 35–53
https://doi.org/10.1080/19475705.2021.2013960

Progressive destabilization and triggering mechanism analysis using multiple data for Chamoli rockslide of 7 February 2021

Wenfei Mao[a,b], Lixin Wu[a,b], Ramesh P. Singh[c], Yuan Qi[a,b], Busheng Xie[a,b], Yingjia Liu[a,b], Yifan Ding[a,b], Zilong Zhou[d] and Jia Li[a,b]

[a]School of Geoscience and Info-Physics, Central South University, Changsha, China; [b]Laboratory of Geo-Hazards Perception, Cognition and Predication, Central South University, Changsha, China; [c]School of Life and Environmental Sciences, Schmid College of Science and Technology, Chapman University, Orange, CA, USA; [d]School of Resource and Safety Engineering, Central South University, Changsha, China

ABSTRACT

A catastrophic rockslide occurred on 7 February 2021 in Chamoli area in the high Himalaya. In the absence of field data, multiple satellites data of decade span have been used to investigate and understand the progressive destabilization of rockslide body. A 3D geometric model was developed using geospatial information about geology, terrain, and ice cover to understand the triggering mechanism. Several causes are uncovered as: the pronounced long-term change of land surface temperature facilitated local permafrost degradation and led to ice cover shrinking since 2010; the occurrence of ice avalanche nearby in 2016 accompanying with sidewall-to-bedrock fracturing enhanced the ice segregation beneath the rockslide body; and the development of side cracks in early February 2021 led to dropping of side support and percolating of surface water. Heavy precipitation several days before favoured the destabilization, top-corner cracks developing and top-side bergschrund breaking abruptly two days before, and ice strength reduction owing air temperature rising few hours before the event triggered finally the rockslide. The frequent disasters such as cloudburst, extreme precipitation, landslides, and snow avalanches responding to global warming and climate change in the Himalayan region needs immediate attention to the chain-like geohazards and collaborative observation with satellites and other platforms.

ARTICLE HISTORY
Received 19 July 2021
Accepted 29 November 2021

KEYWORDS
Chamoli rockslide; multiple source satellite data; geospatial information; development process; geometric model; rockslide triggering

1. Introduction

In the high mountain areas worldwide, the depleting of snow/glaciers and permafrost freezing-thawing process, being considered as an important mechanism to induce slope

CONTACT Lixin Wu, wulx66@csu.edu.cn

failures, such as landslides/rockslides, rockfall, ice and rock avalanches (Haeberli 1997; Davies et al. 2001; Gruber and Haeberli 2007; McColl 2012; Krautblatter et al. 2013), are evidence of global warming and climate change. The effects of liquefied water, low-friction surfaces and steep topography were identified as critical driving factors enhance the mobility of large rock-ice avalanche volume (Schneider et al. 2011). However, identifying potential rock/slope failure and predicting the event, which could be related to a group of driving factors, are still very difficult, in the absence of field data and geophysical information especially in the high mountain areas.

In recent years, the utility of satellite-based remote sensing data offers valuable tools for better understanding and qualifying the natural hazards process in high mountain areas (Ambrosi et al. 2018; Kirschbaum et al. 2019). For instance, due to lack of sufficient eyewitness and monitoring system, Champati et al. (2016) have investigated the causes and consequences of Kedarnath 2013 disaster utilizing the multiple satellite data, including precipitation, snow cover and digital elevation models, and have revealed that the series of landslides and lake outburst are the main causes in the Himalayan region. On the basis of satellite remote sensing, numerical modelling and field investigations, Kääb et al. (2018) have reported two adjacent glaciers in the western Tibet in the months of July and September 2016 and found the collapse was caused by climate- and weather-driven external forcing, which massively reduced the basal friction connected to subglacial water and fine-grained bed lithology. Leinss et al. (2021) identified several Glacier detachments and rock-ice avalanches occurred between 1973 and 2019 in the Petra Pervogo range, Tajikistan using Landsat archive, Sentinel-2 images and the ASTER imaginaries.

On 7 February 2021, at 4:51 UTC (10:21am Indian Standard Time [IST]), a huge block of mountain rock covered with ice got detached from the north slope of Ronti Peak and fell down in the valley from 1800 m height (Figure 1). The detached rock and ice rapidly transformed into debris flow and generated a cascade of events, which consequently swept away the unfinished Tapovan-Vishnugad Hydropower project and caused more than 200 deaths or missing (Shugar et al. 2021; Rao et al. 2021; Pandey et al. 2021; Renoj et al. 2021). Due to high-altitude and steep topography, it was difficult to get ground information from the top of the mountain above 5000 m asl. Pandey et al. (2021) carried out helicopter survey on 12 February 2021 and took few photographs which provided valuable information around the rockslide areas. The extremely steep slope, long-term air temperature rise, regional climate change and related disturbance in cryosphere as well as heavy precipitation several days before the event were thought to be the causes of the rockslide (Shugar et al. 2021; Pandey et al. 2021; Renoj et al. 2021). We have used multiple satellites observations (optical and microwave) and a three-dimensional geometric model based on geospatial information to investigate the development process and to understand the causes of the triggering mechanism of this deadly rockslide in the absence of detailed ground observations.

2. Topography

The Chamoli area, as a part of the the high Himalaya, mainly consists of high-grade metamorphic rocks (Valdiya 1980) and the area around the Tapovan-Vishnugad

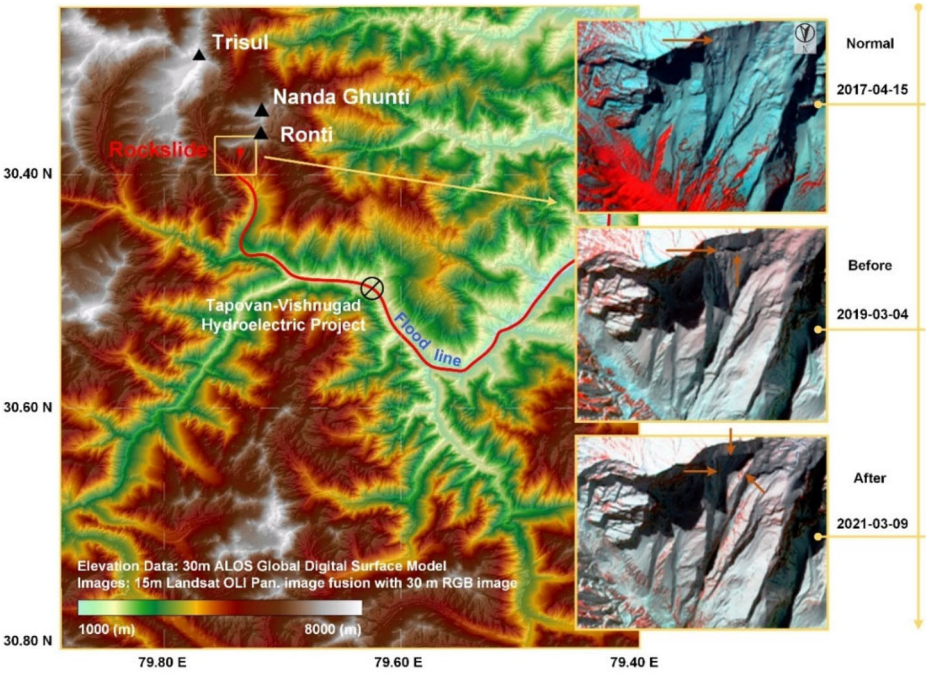

Figure 1. The location map of Chamoli rockslide on 7 February 2021. In the right panel, three fusion images from Landsat-8 show the regional steep topography and location of the rockslide on 15 April 2017, 4 March 2019 and 9 March 2021, respectively.

hydropower station about 20 km downstream is dominated by amphibolite facies, psammitic schist and gneisses (Heim and Gansser 1939; Valdiya and Goel 1983), of which the non-tectonic joints are usually much developed (Nichols 1980) and their stratified structure are easy to be affected by glaciation, deglaciation and neotectonic process (Sahoo et al. 2000; McColl 2012). The elevation range of the rockslide body is about 5,600 masl (Figure 2a), which is of high potential energy for mass movement and landslide. The actual bergschrund was close to the mountain ridge (with distance of about 273 m), which illustrates the sheard nature of the source rocks to likely condition of the faliure (Shugar et al. 2021). There were many glacier spurs existing on the slope (Figure 2b), where the permafrost degrades usually faster and deeper compared to a straight slope (Noetzli et al. 2007). Longterm changes of air temperature had impacted significantly the permafrost layer along the slope.

The rock mass at the northern slope of the ridge appears to be stratified, and the west adjacent surface of the slope appears to be relatively lower (Figure 2b). It seems that bedrock instabilities have developed progressively from lower altitudes upwards (Fischer et al. 2013), and some rockslides or ice avalanches might have occurred nearby in the recent past, but no records are available. Before this event (7 Feb. 2021), slope angle of the sliding body surface was about 40° (Figure 2c), which is a little higher than the sliding threshold of 37°. The sliding body can be considered as a "steep" slope (Gruber and Haeberli 2007), on which most of seasonal snow overburden are likely to fall down and thin snow cover will be easily melted during warm summer.

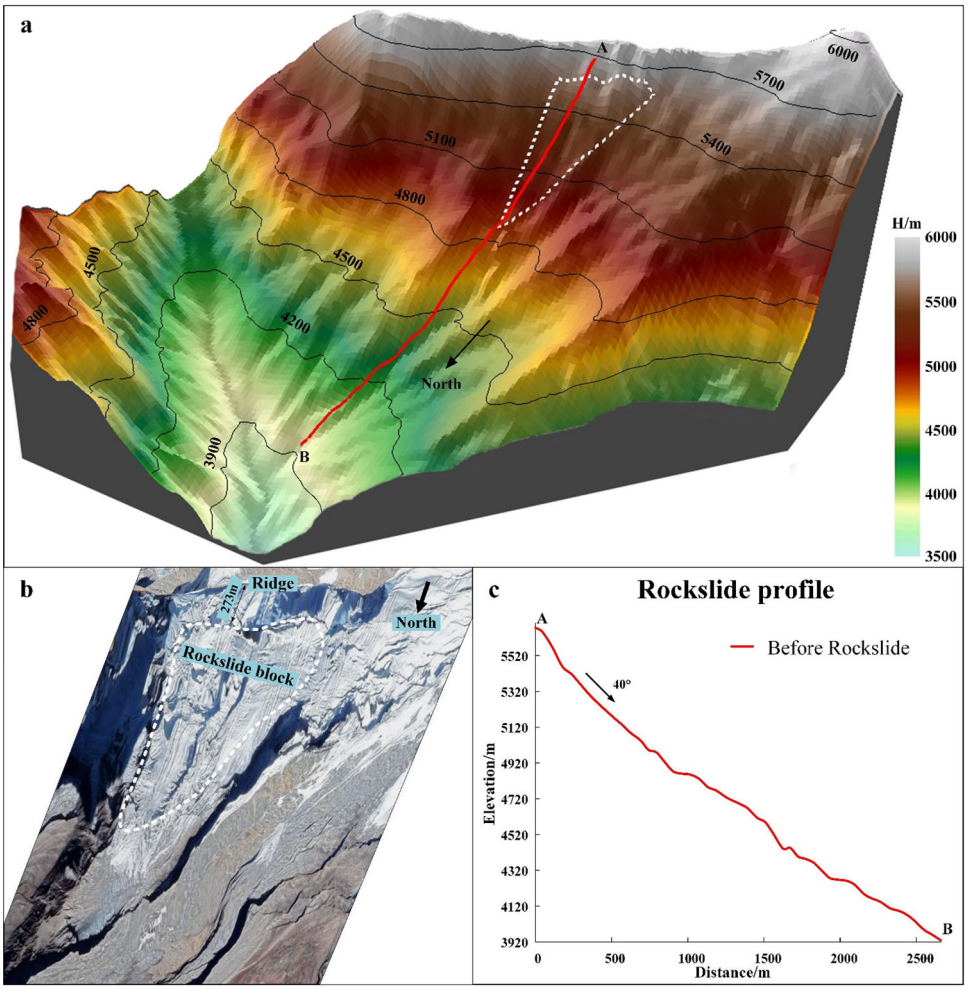

Figure 2. The topographical conditions around the rockslide place. **a**. Digital elevation model from ALOS (Advanced Land Observing Satellite) shows the rockslide place, and white dashed polygon illustrates rockslide area; **b** Google earth image of 2017, shows stratified rock mass; **c**. Rockslide profile ('AB') is shown with red colour (**a**).

3. What changed gradually in a decade

3.1. General LST rising in 2013–2021

In the last few decades, the Himalayan region was experiencing a significant rise in land surface temperature (LST) (Sabin et al. 2020), especially during pre-monsoon and winter season (Gautam et al. 2009; Negi et al. 2018). The changes in LST in Chamoli and its surrounding areas is observed using AMSR-2 microwave brightness temperature (MBT) data (89 GHz horizontal polarization) 2013–2021. Physically, the observed MBT of an object is related to its physical temperature and surface emissivity (Ulaby and Long 2014). If surface composition and moisture are considered no change in the same month, for example in the months of January and February of each year, the MBT varies only with LST. The MBT data from satellite AMSR2 with

a spatial resolution of 5 km was superimposed with a true colour image from satellite Sentinel-2 with a spatial resolution of 10 m, compared with the two typical homogeneous pixels, being representative rock surface (R) and vegetation (V) of different land coverages, were considered (Figure 3a). In particular, the homogeneous pixels are presented to meet the following two criteria: (1) the pixels are basically of the same type of land cover from their texture in the true colour image; and (2) the locations of the pixels are close to the location of the rockslide. Besides, the pixel containing partially the rockslide was also selected and labelled as key pixel (K) (Figure 3a). We computed the monthly average MBT of all the typical pixels for the months of January, February and October of each year 2013–2021 using approach of Qi et al. (2021).

As shown in Figure 3b, c, e and g, all the three types of pixels show similar MBT variations in the months of January and February 2013–2021, with pronounced changes in 2018–2020 and an increment in 2021. Considering the surface composition remains same and moisture no change during this period, the microwave emissivity of these pixels can be assumed to be unchanged accordingly, thus the observed MBT variations are caused mainly by the change of LST. The MBT over the study area (K-pixel in Figure 3a) shows significant high-and-low variations during 2013 to 2021 (Figure 3g). Such dramatic MBT changes of K-pixel implies unusual thawing–freezing–thawing behaviour during 2018–2021, that could be a potential active factor of the rockslide. In addition, variations of the average monthly MBT of K-pixel during 2 years before rockslide suggests that the LST in the month of February 2021 was a little higher compared to the month of February 2020 (Figure 3d), which might be a potential cause of the triggering of 2021 rockslide event.

However, sometimes the change in surface composition could also cause the variations in observed MBT. To further evaluate the impact of changes of surface composition in different years, the land cover of each pixel is classified using remote sensing data of Lansat-8 and Sentinel-2 from 2013 to 2021. The surface composition over pixel R1 in the month of January, was filled with $80-85\%$ rock, showing $15-20\%$ of pixel was filled with snow coverage (Figure 4). The rock percentage kept relatively stable during the periods 2013–2021. Similarly, the rock percentage in the month of February was less compared to the month of January showing approximately no change during the periods 2018–2021. Therefore, the observed variations of MBT (Figure 3c) during the periods 2013–2021 was mainly caused by LST. In general, the rock percentage of pixel R2 is less than those of pixel R1 due to higher snow coverage at higher altitude during winter season. The pronounced changes in rock percentage were observed during January and February 2013–2021. The correlation between the variations of rock percentage and the change in MBT (Figure 3e) is found to be poor, which reflects that the observed MBT changes over pixel R2 was not caused mainly by surface composition. The selected vegetation pixels V1 and V2 show about 50% of the area were covered by vegetations, slight variations in vegetation cover shows the areas were relatively stable as well, which is not consistent with the changes in MBT (Figure 3b).

Very a few vegetation was observed during summer in K-pixel, and the changes of area percentage of rock or dry snow/ice in K-pixel is sensitive to the MBT of K-pixel.

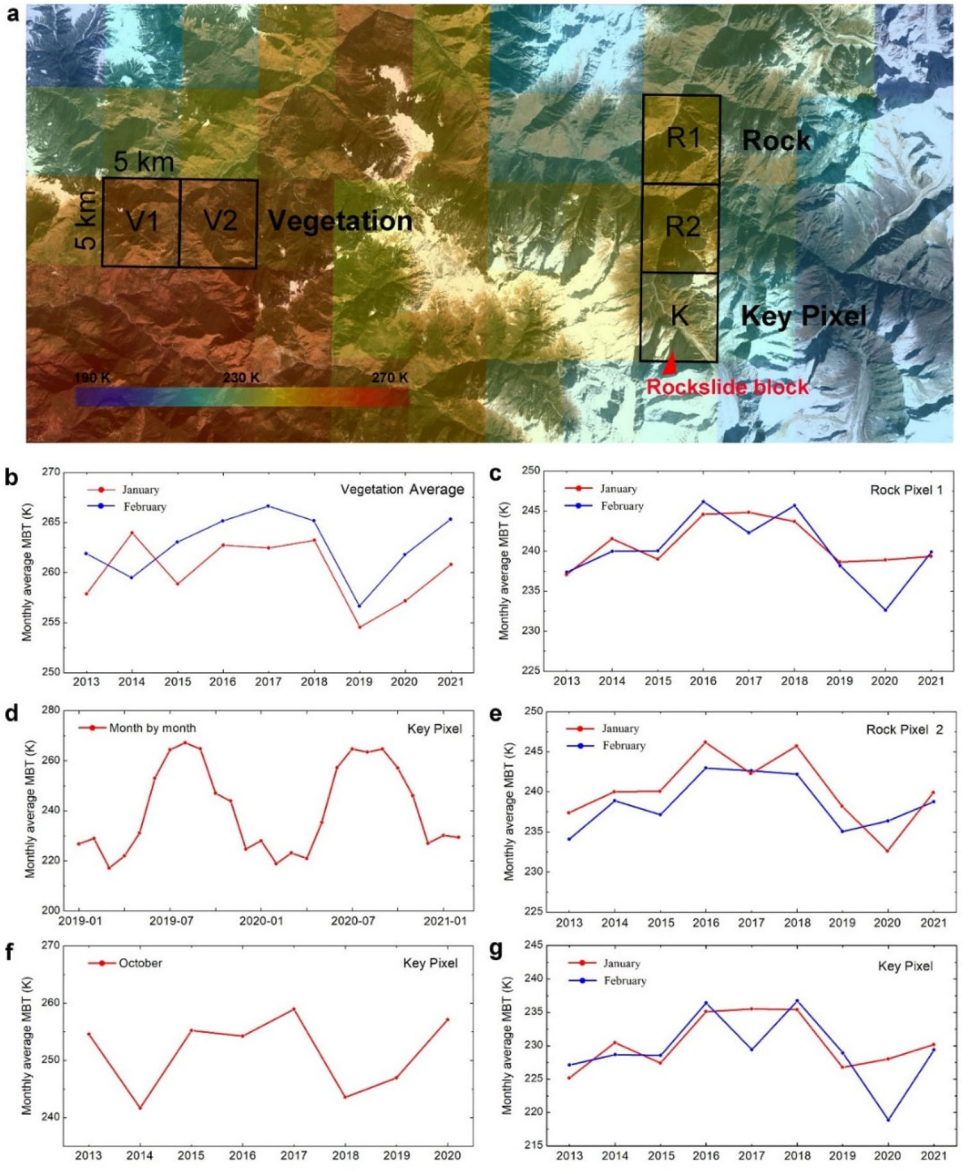

Figure 3. Schematic diagram of typical pixels and its monthly average MBT. **a**, selected typical pixels are marked with black boxes: Rock surface (R), Vegetation (V), and Key pixel (K) covering the rockslide; **b**, Monthly average MBT of the two V-pixels in January and February 2013–2021; **c**, Monthly average MBT of the R-pixel-1 during January 2013 to February 2021; **d**, Monthly average MBT of the K-pixel during January 2019 to February 2021; **e**, Monthly average MBT of the R-pixel-2 during January 2013 to February 2021; **f**, Monthly average MBT of the K-pixel in October 2013–2021; **g**, Monthly average MBT of the K-pixel in January and February 2013–2021.

Comparing Figures 3g and 4, variations of observed monthly average MBT during January and February show a good correlation to the variations of rock percentages in the months of January and February, respectively, which suggests an increase in rock percentage, or the decrease in dry snow/ice percentage, to the increase in MBT.

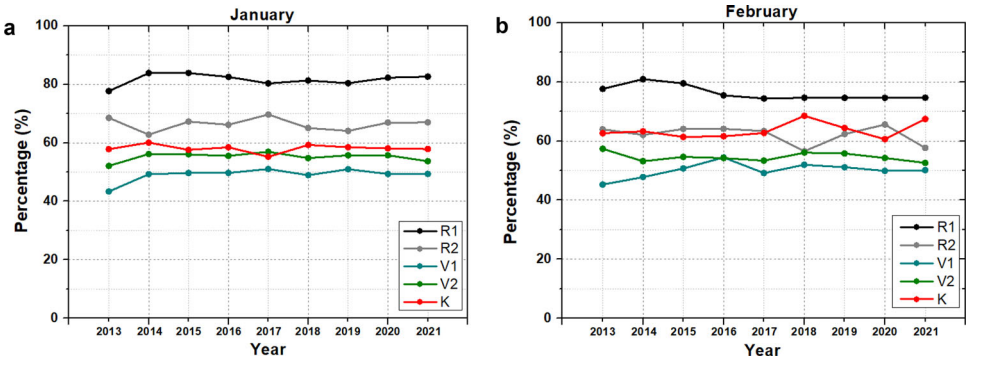

Figure 4. Changes in surface composition of selected pixels in the same month of different years. **a**, the variations in January of each year; **b**, the variations in February of each year. Black and grey lines represent the rock percentage in pixels R1 and R2 respectively, the olive and dark green lines represent the vegetation percentage in pixels V1 and V2 respectively, the red line represents the rock percentage in Key pixel.

However, physically the microwave dielectric constant of rocks from 4 to 10, while the dielectric constant of dry snow/ice is <3.2 in microwave frequency range (Ulaby and Long 2014). With the physics of remote sensing and the constant physical temperature, the higher values of dielectric constant in microwave frequencies corresponds to the lower MBT. Thus, theoretically the increase of rock percentage or the decrease of dry snow/ice percentage decrease the MBT, showing an inverse relation to the observations (Figures 3g and 4). Thus, we can conclude that the variations of MBT of K-pixel is mainly caused by the changes in LST. With the increase of LST, the area percentage of dry snow/ice is decreased and correspondingly area percentage of rock increased.

In addition, the skin temperature (SKT) derived from ECMWF ERA5 climate reanalysis datasets are used to study temperature variations before and after the event. By selecting a pixel with a size of 0.1° by 0.1° within the location of rockslide, the regional mean of SKT over time is calculated. The change of SKT 70 days before the rockslide event shows dramatic fluctuations with average amplitudes of 10 K, while the background values show a relatively weak fluctuations with average amplitudes of 5 K only (Figure 5). Such variations show intensive freezing–thawing cycles were expected decades of days before the event and consequently facilitate the destabilization of rockslide. In addition, the SKT during 5 days before the rockslide shows a dramatic decrease–increase fluctuation. With the dramatic decrease of SKT from 3 to 4 February 2021, the water infiltrated into fractures prior to the event was frozen further and ice segregation effect was increased significantly. The continuously increase of SKT from 4 to 7 February 2021 reduced the shear resistance that provided favourable mechanical conditions for the final destabilization of the rockslide body.

3.2. Ice cover shrinking since 2010

To investigate the ice or glacier shrinking with LST rising, cloud free satellite images for the month of October (being less snow fall) of each year for the periods

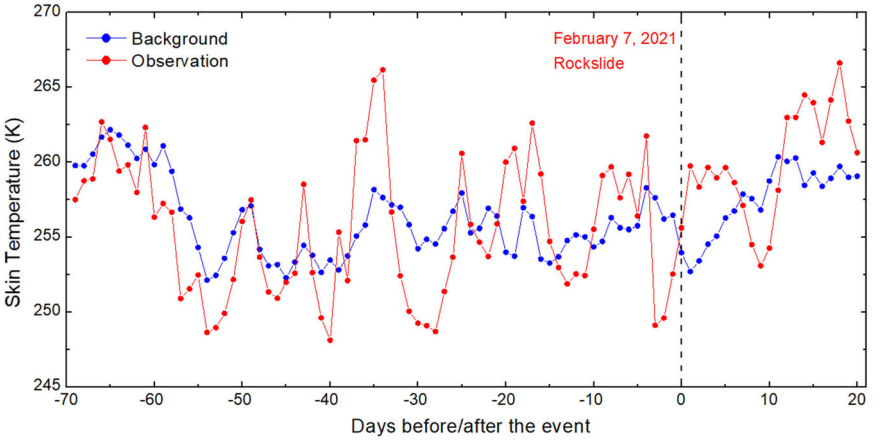

Figure 5. Skin temperature before and after the Chamoli rockslide event. The red line exhibits the most recent observation of SKT before and after the event, while the blue line shows the background SKT from 2013 to 2021.

2002–2020 were considered, the mean LST were above 0 °C in the month of October (Renoj et al. 2021). The ice cover in whole study area started to shrink in 2010 and declined from 81.5% to 13.9% in 2017 (Figure 6), increased again in 2018 and reached to 33.7% in 2019, but declined with the minimum to 6.7% in 2020 associated with the changes in MBT during 2009–2020 (Figure 3f). The ice cover inside the blue dashed rectangular began to decrease in 2012, which is a little later compared to the whole study area due to difference in elevation. This shows that the rock slope gradually exposed to the warming air. Inside the orange dashed triangle, the reduced ice cover from 2012 to 2016 located mainly at the lower part, provided support to upper rock mass. For the rockslide body itself, most surface was covered by ice and kept relatively stable before 2020, but dramatically decreased to 31.7% in 2020. About 13.6% of the surface of rockslide body exposed in 2017, which implies that some of the melting water from ice cover might have percolated into the bedrock of rockslide body, and consequently weakened the mechanical property of shallow bedrock with increasing pore-water quantity and joints-water level on the bottom of bedrock. Followed with two years of low temperature in 2018 and 2019 (Figure 3f), the percolated water was frozen again and activated the ice segregation effect (Taber 1930) in the rockslide body. In the meantime, the frost heave (Hallet 1983; Walder and Hallet 1985) might have also enhanced fracture density in bedrock. In October 2020, with a higher temperature, almost 70% of the rockslide surface got exposed, which indicates large amounts of available water further percolated into the bedrock, and the followed freezing behaviour and ice segregation from November 2020 to January 2021 was enhanced unprecedentedly. Therefore, it is convincible that the climate changes during the past years had facilitated the ice melting and permafrost degradation, and consequently led to glacial debuttressing, which is defined as the removal of side support from adjacent glacier ice (Ballantyne 2002; McColl 2012). Consequently, the weakening and slow withdrawal of side support since 2020 reduced the slope stability.

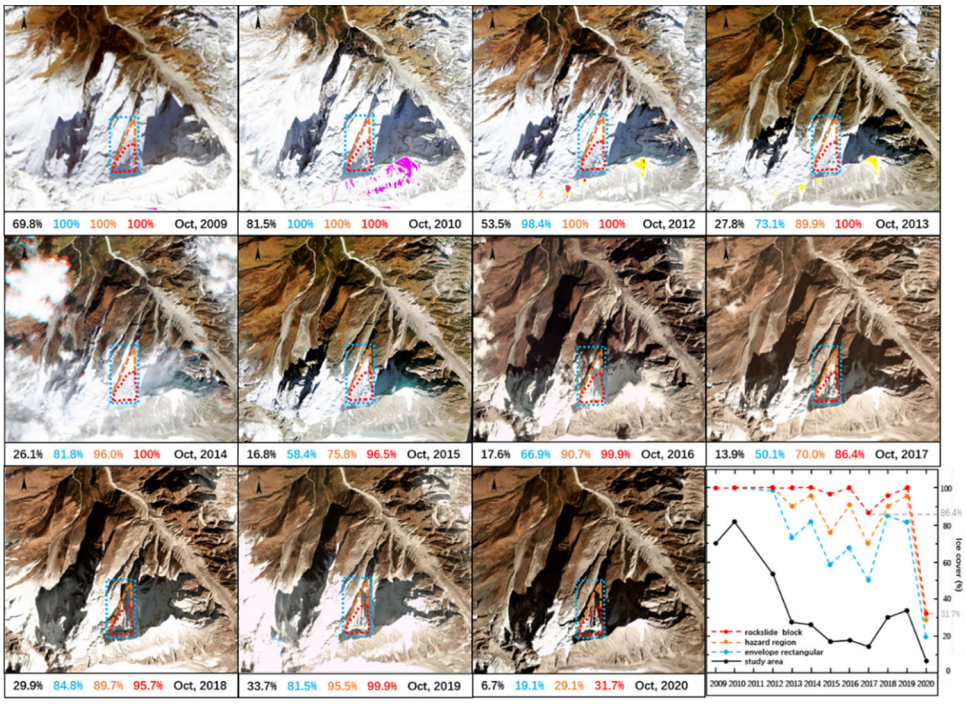

Figure 6. Changing ratio of ice cover in the core areas of rockslide in 2009–2020. (Planet's image of October 2011 is not taken due to intense cloud cover). The total area of the study area is about 36 km^2, and the blue dotted rectangle with area 1.5 km^2 represents the envelope of sliding zone, shown with orange dashed polygon; the rockslide place is shown with red doted polygon. The values with black, blue, orange and red colour represent the area percentage of snow-ice cover in the entire zone, blue rectangle, orange polygon and red polygon, respectively. Due to the incompleteness of a certain band in Planet sensor, local anomalies did exist in some images.

3.3. Adjacent ice avalanche in 2016

In contrasting to the Sential-2 images of 19 September and 9 October 2016, an ice avalanche (yellow dotted area) had occurred (Figure 7), as a result of the climate change. The west part of the bedrock of the rockslide body exposed after the closely adjacent ice avalanche, and the solar radiation on the exposed bedrock could be increased, which enhanced the water seepage and freezing–thawing cycle. In 2017, 13.6% (i.e., 86.4% ice cover) of the surface of rockslide body (Figure 6) exposed that accelerated the melting of ice cover, that must have percolated into the bedrock and consequently enhanced the volume of pore-water and joints-water level in bedrock. Thus, it could be expected that the percolating water through the joints enhanced a lot in the bedrock after the 2016 ice avalanche and ice melting in 2017.

3.4. Bedrock fracturing since early 2017

The local stress field was disturbed by the ice avalanche in 2006, which was located in the west of closely potential rockslide body, through glacial buttressing and stress-release fracturing that weakened the side support. This led to enhancement of the

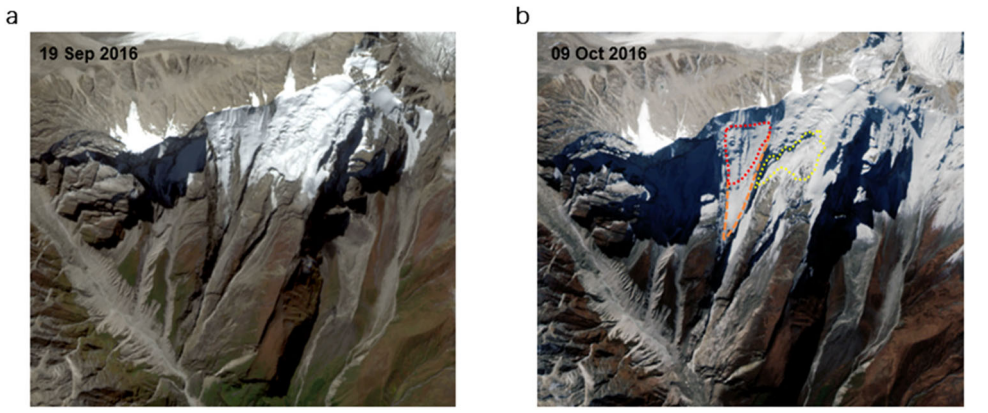

Figure 7. The ice avalanche (yellow doted polygon) occurred in study area in 2016. **a**, 19 Sept 2016 image before the avalanche; **b**, 9 Oct 2016 image before the avalanche.

instability of the rockslide body, and facilitated the appearance of cracks on its topside in 2017 (Figure 8). For the enhanced ice melting and permafrost degradation during the periods 2013–2017, the bedrock of the rockslide body lost its strength gradually and fractures were developed as pathways of subsequent water percolation. In that frost heave could enhanced the density of micro fractures and its growth in bedrock (Hallet 1983; Walder and Hallet 1985), the low LST in 2018 and 2019 (Figure 3) could have enhanced the ice cover on the rockslide body significantly (Figure 6), and the ice segregation was activated and enhanced due to available pre-percolated water with the deep-ward movement of freezing front. Consequently, the buttering of ice above the rockslide body was relatively increased in 2018 and 2019, the topside crack produced in early 2017 was developed quickly and a horizontal crack of width 50 m about with sharp edges, even with snow cover, appeared clearly on 24 October 2018 (Figure 8).

In the month of October 2020, with a higher LST (Figure 3f), 68.3% (i.e., 31.7% ice cover) of surface of the rockslide body got exposed (Figure 6), which indicates large amount of available water might have further seeped into the bedrock through topside cracks, west side fractures and the widening bergschrund. Hence, the rock joints or potential failure surfaces might have satrured. In the following winter months with low temperature from November 2020 to February 2021 (Figure 3d), the frost heaving by ice segregation in bedrock joints together with the volume-expansion pressure at deep part of bergschrund, where the shallow space was sealed due to freezing of water and a closed system was produced, were enhanced unprecedentedly. Two days prior to the rockslide, the size of the bergschrund expanded quickly (Figure 8), and two top-corner cracks produced abruptly at the west and east corners of the rockslide body, respectively, get connected to the bergschrund at the topside crack. The pattern of potential rockslide body appeared clearly in Sentinel-2 image on 5 February 2021. It is obvious that the rockslide body had reached to a critical stage, and any other favourable factors were able to trigger the rockslide. The continuous snowfall on 2–6 February 2021 (Pandey et al. 2021) could have led to the decrease of shear strength of rockslide body.

4. Progressive destabilization and final triggering

4.1. 3D Geometric model of rockslide body

From Sentinel-2 optical images we estimated the bounding of the rockslide body. Aspect map produced from digital elevation model (ALOS-30m DEM) and optical images downloaded from Planet Labs17 are used to characterize the spatial relationship of the faces of rockslide body (Figure 9a). The west side face (face C) of the rockslide body is assumed to be approximately parallel to the adjacent faces (i.e., face L3-2 and face L4), so that we can use terrain factors of the adjacent faces to approximate face C. The slope of face C is about 35.1° with northeast aspect (30°). The east side face is assumed to be consistent with face S1 with northwest aspect (50°). The slope of the top face (face L2-1) is about 40° with north aspect. According to the spatial relationship between these side faces (shown in Figure 9c,d) we presumed the rockslide body as an irregular hexahedron object, whose thickness is referred to earlier study obtained from aerial observations (Pandey et al. 2021).

We noticed also a strip-shaped ice block (red dotted polygon in Figure 9a) remain staying on the slope after the rockslide event, which indicates that the upper sliding body might have experienced a lifted flying over the lower ice block. The scar of the rockslide, stratified rock surfaces and stepped faces between the stratified layers (Figure 9d), which is also observed from close looking by helicopter (Renoj et al. 2021), an irregular shape of rockslide body is outlined, and a 3D geometric model of the rockslide body was constructed as an irregular hexahedron object with volume about 18.797 million cubic meters. By simplifying the boundary conditions of the rockslide body, a conceptual mechanical model is further developed (Figure 9b).

4.2. Progressive destabilization

Considering the geometric characteristics of the rockslide body (Figure 9) and the shrinking process of ice cover (Figure 6), the progressive destabilization of rockslide body is shown in Figure 10. When the snow line reached up to the lower part (ice block) of the rockslide body in 2017, surface melting water was likely to percolate into the bedrock and the opened ice-filled joints. The percolating water may have frozen again, and the process of ice segregation could have produced the frost heave (Hallet 1983; Walder and Hallet 1985, 1986) accompanying with the upward displacement of overburden bedrock and the developing of a crack at the top-side of the rock volume. Later, with the freezing-and-thawing cyclic process during 2017–2021, more ice could have filled primarily in the bottom that may have produced rock fractures and joints, giving rise to large fracturing in rock mass. Large amount of snow might have filled in the bergschrund that could enhance the freezing and thawing effect. During thaw cycles, snow melts during summer season, freezes again during winter that change the stress because of volume expansion, which may enhance stress to the frozen rock mass and assist the destabilization of rockslide body. Consequently, the crack got expanded and developed completely and got detached. With the connection of the bottom joints and the bergschrund, the ice segregation effect got enhanced and favoured the lifting of bedrock, which eventually lead to the destabilization of the rock slope.

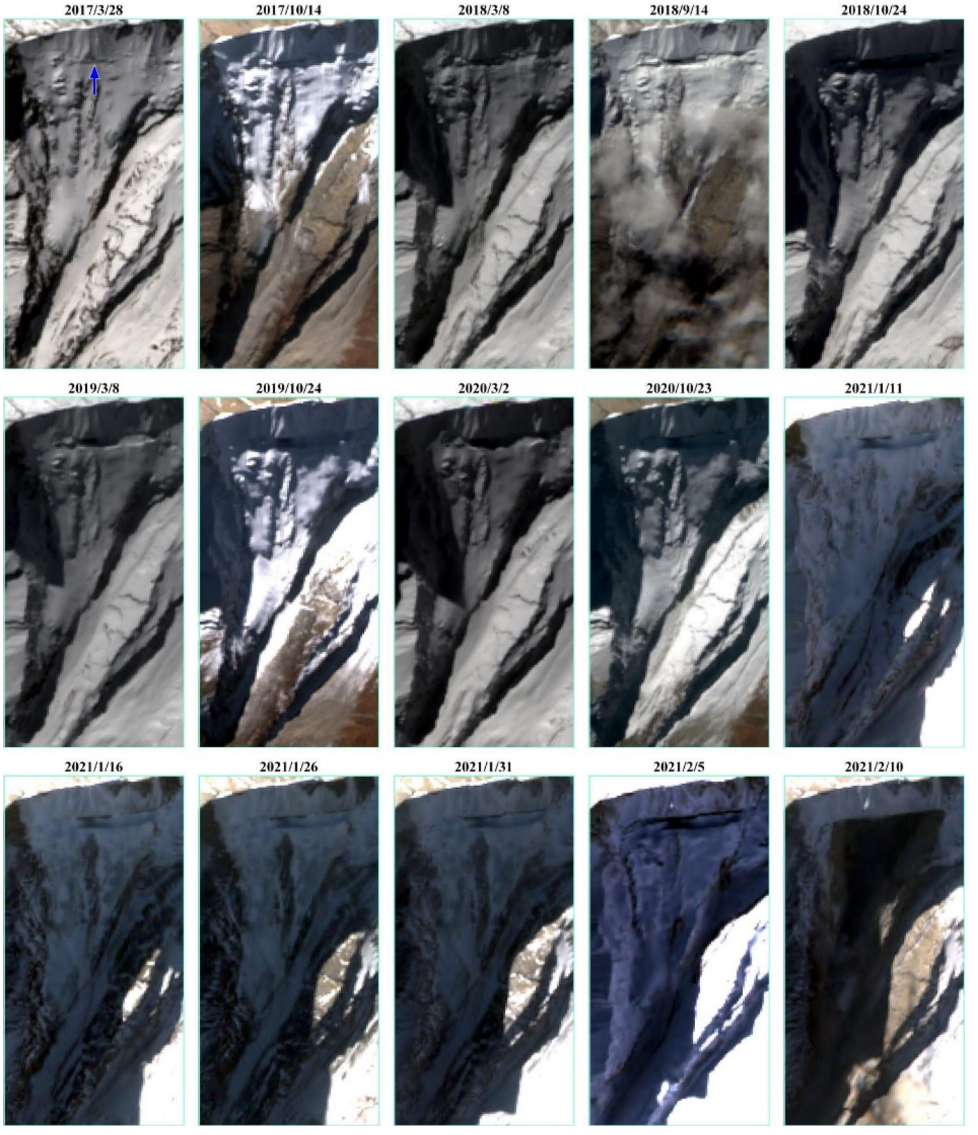

Figure 8. Sentinel-2 images of the rockslide place during March 2017 to February 2021. These images are picked out from all available images in each March and October or September 2017–2020, and all those from January 11 to February 10, 2021, inconsideration of less cloud and nice quality. The topside crack or bergschrund was visible on 28 Mar. 2017 (pointed by blue arrow). With the time going, the length and width of topside bergschrund developed gradually. On February 5, 2021, 2 days before the rockslide, the top-side bergschrund was broken abruptly, and a triangular rockslide body was clearly outlined by three opening cracks at the top, left and right side, respectively.

4.3. Final triggering

The ultimate balance theory was applied to analyse the destabilization of the rockslide. The boundary conditions of the rockslide body are simplified, and a three-dimension mechanical model is presented (Figure 11a). The mechanical forces related

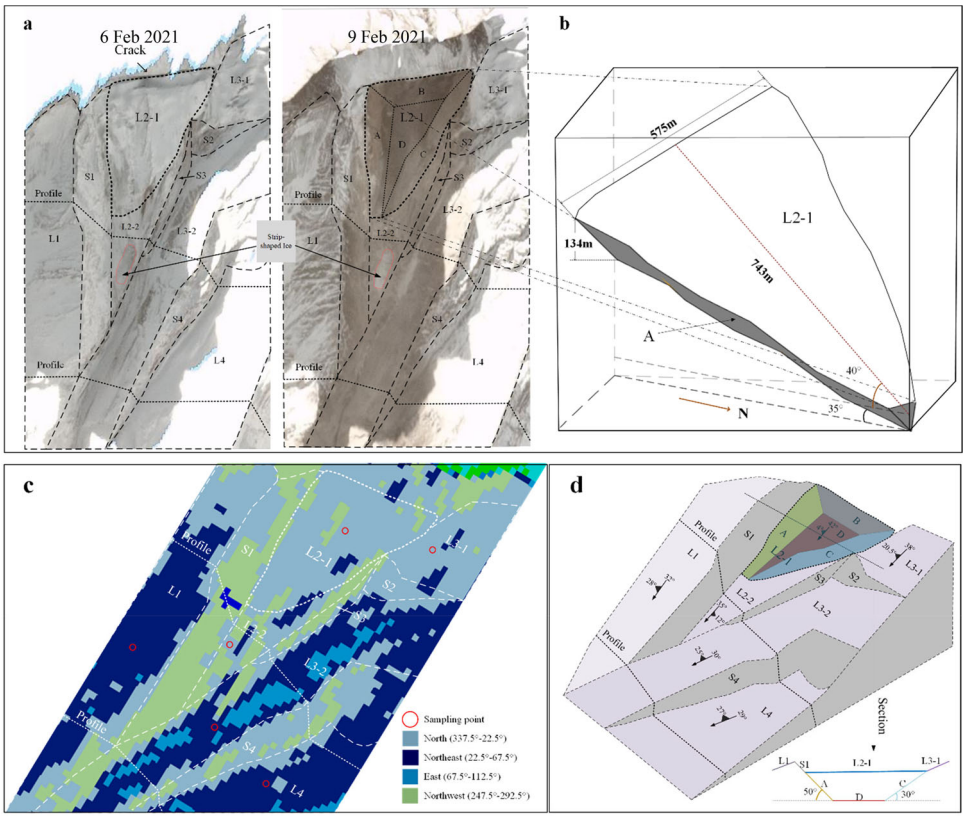

Figure 9. 3D geometric model and characteristics visualization of the rockslide body. **a**, Optical images before (6 Feb 2021) and after (9 Feb 2021) the rockslide event, data from Planet's Labs; **b**, Eastside view of the three-dimensional (3D) model of rockslide body; **c**, Inclination map of terrain surface corresponding to the area in a; **d**, Spatial relationship between the rockslide body and its adjacent surfaces in the aspect direction. Surface A, B, C, D and L2-1 enclose together the sliding body; L2-1 and L3-1 are the glacial surfaces of the 2021 sliding body and the 2006 ice avalanche body, respectively; L1, L2-2, L3-2 and L4 are stratified rock surfaces; S1, S3 and S4 are stepped faces between stratified layers; S2 is the fracturing face of the 2006 ice avalanche, the pink dotted polygon show a remained strip-shaped ice body.

to a layered rock mass on a slope are divided as shear force (F_s) and shear resistance force (F_r), which try to pull or hold the rock mass on the slope. Thus, the stability of the rock slope can be obtained theoretically as:

$$f = \frac{F_r}{F_s} = \frac{F_{3e} + F_{3w} + F_4 + F_5}{(F_1 + F_2)\sin\theta + F_6} > 1.0 \tag{1}$$

where f is the stability coefficient. The shear resistance forces in joints, including F_{3e}, F_{3w} and F_4, is mainly determined by the creeps and fractures of ice (Paterson 1994), the failure of rock–ice contacts (Krautblatter et al. 2013), the friction along rock–rock contact (Barton and Choubey 1977) and the fracture of intact rock bridges (Kemeny 2003); while the force on bergschrund, F_5, is mainly influenced by ice–rock adhesion (Ryzhkin and Petrenko 1997); and F_6 is determined by the closure features

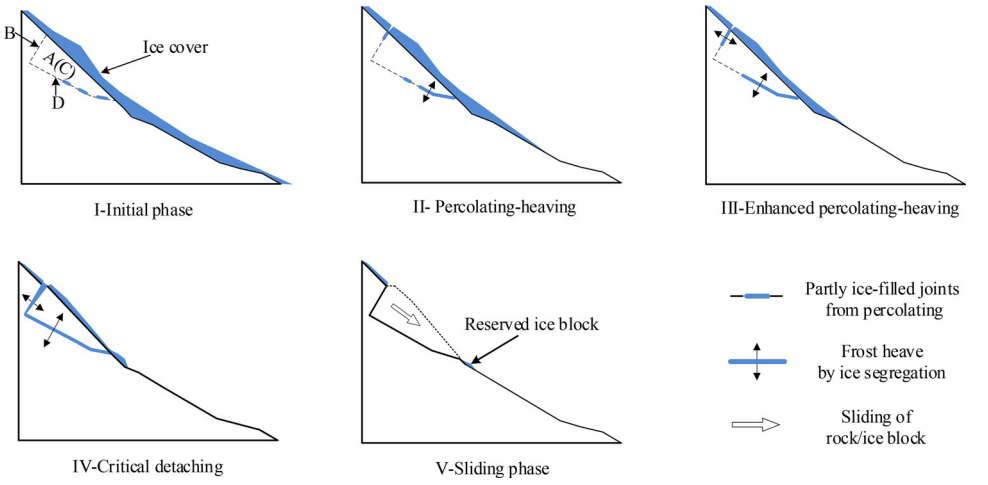

Figure 10. A schematic diagram of the progressive destabilization of the rockslide body owing to percolating, heaving, and detaching actions.

of local rock–ice system (Taber 1930). Experimentally, the shear resistance in joints shows a reduction trend with the rise of temperature (Krautblatter et al. 2013).

The general stability evolution of the rockslide body in 2013–2021 is shown in Figure 11b–d. Since the ice avalanche in 2016 (Figure 7) and bedrock fracturing in 2017 (Figure 8) could have reduced the shear resistance forces significantly, the shear resistance curve shows two significant falls accordingly. While during one year before the rockslide, the stability depended largely on LST variations and probable volume expansion pressure. During several days before the rockslide, precipitation (Jiang et al. 2021) lead to the rising of F_2 and decreasing of f. In addition, two top-corner cracks produced along the east and west sides of the sliding body and connected with the topside bergschrund on 5 February 2021, which might have decreased the shear resistance significantly. Besides, the higher the temperature, the lower the ice-bonding force (Kemeny 2003) and ice shear strength (Fish and Zaretsky 1997). The hourly air temperature at rockslide location (30.38°N 79.73°E) from 1 to 7 February 2021 is shown in Figure 11d (Jiang et al. 2021). In 24 h before the event (10:21 am, IST), the air temperature declined from −10 to −22 °C in the first 12 h, with which the effect of frost heave was expected to be enhanced correspondingly. Afterwards, the air temperature rose monotonously from −22 to −2.5 °C in the latest 12 h, thus the significant reduction of the ice strength, including the ice-bonding force at bergschrund and the ice shear strength in potential failure surfaces, would have promoted the final triggering of the rockslide. Thus, during several days to a few hours before the rockslide, approximately all forces applied on the rockslide body were favour for the destabilization, especially at the last moment in the 7 February morning. Therefore, the increasing shear force coupling with the decreasing shear resistance facilitated dynamically the progressive destabilization of the rockslide body as:

$$f = \frac{F_{3e}\downarrow + F_{3w}\downarrow + F_4\downarrow + F_5\downarrow}{(F_1 + F_2\uparrow)\sin\theta + F_6\uparrow} \rightarrow 1.0 \tag{2}$$

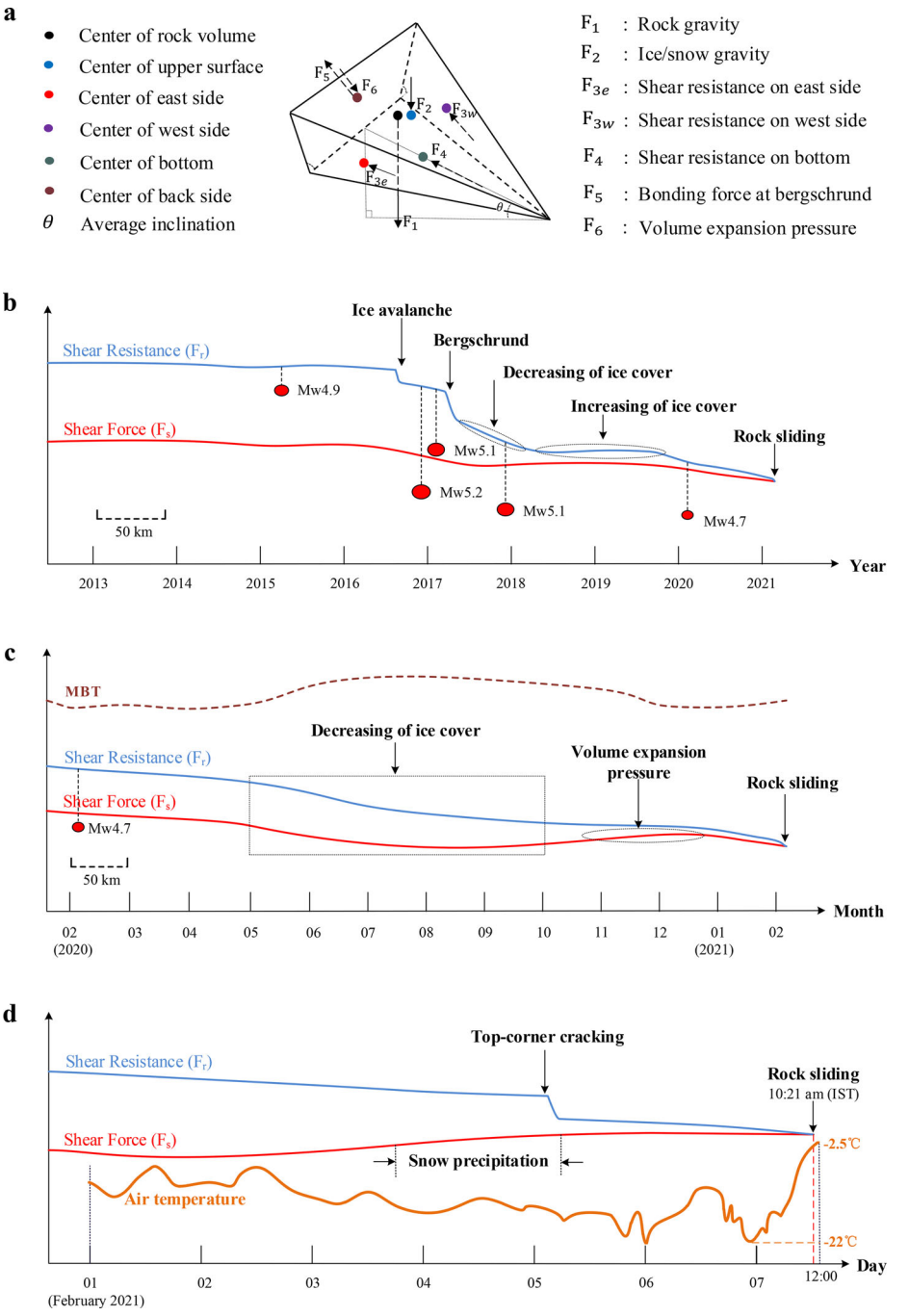

Figure 11. Mechanical equilibrium system and progressive destabilization of the rockslide body. **a**, Schematic diagram of applied forces on the rockslide body; **b**, Conceptual evolution of shear force and shear resistance in 2013–2021, the red dots represent the earthquakes (USGS) of potential disturbance to shear resistance, the black dotted line shows approximately the distance between the epicentre and rockslide; **c**, Conceptual evolution of shear force and shear resistance from March 2020 to February 2021; **d**, Conceptual evolution of shear force and shear resistance in the last week from 1 to 7 February 2020.

Although the long-term trends of increasing high-mountain slope failures could be attributed to climate change (Bessette-Kirton and Jeffrey 2020), the general attribution of single event remains largely elusive (Shugar et al. 2021). Some researchers grouped the factors that result in the paraglacial rock-slope failures into three types: preconditioning, preparatory and triggering factors (Glade and Crozier 2005; McColl 2012). Climate changes, glacial erosion, glacial debuttressing, rock stress redistributions and jointing as well as seismicity, are recognized as factors that could reduce the stability, and change the slope from a 'marginally stable' to 'actively unstable' state. Thus, to evaluate the stability of rock-slope in high-mountain areas, the perception and recognition upon the factors mentioned above is always necessary.

In general, the Chamoli rockslide could be attributed to three specific factors: (1) the snow/ice cover on the slope, shown with orange and red polygons (Figure 6), had experienced a 'cyclic' evolution due to global warming, i.e., shrinking gradually from 2012 to 2017, increasing again from 2017 to 2019 and dramatically declining in 2020, of which the process of thawing–freezing–thawing effect was magnified and the ice-water condition inside the slope bedrock is changed significantly. (2) An adjacent ice avalanche has occurred in 2016 (Figure 7), which disturbed the local stress and the thermal conditions in the area of detachment zone. (3) The huge top-side crack acting as the head scarp of the rockslide produced since early 2017 (Figure 8), subsequently reduced the shear resistance of rockslide body and provided a great pathways of water percolation.

5. Conclusions

Supported with multiple satellites data since 2009, we investigated the progressive development of 7 February 2021 Chamoli rockslide and developed a 3D geometric model of the rockslide body based on geospatial information to understand the rockslide triggering. Local LST change for decade, shrinking ice cover since 2010, yearly permafrost freezing-thawing, closely adjacent ice avalanche in 2016, bedrock fracturing since early 2017, and side-support weakening since 2020 are proved to be driving factors, which had all impacted on the development process of Chamoli rockslide and facilitated the rockslide destabilization progressively. Especially, snow fall several days prior to, top-corner cracks developing as well as bergschrund breaking abruptly two days before, and significant rise of air temperature a few hours preceding the rockslide should have provided favourable mechanical conditions for the final triggering of the rockslide.

In addition to understand the progressive destabilization and triggering factors of Chamoli rockslide, the corresponding downstream chain reactions, including the source and process of debris flood, surface deformation, changes in flood plains and water quality as well as the detection and early warning method, could also be investigated and revealed by using satellite images and regional seismic networks (Pandey et al. 2021; Kothyari et al. 2021; Shugar et al. 2021; Jiang et al. 2021; Meena et al. 2021a, b, c; Cook et al. 2021; Rao et al. 2021; Renoj et al. 2021). However, the spatio-temporal data resolution limitations have been a major limitation in the application of remote sensing to high mountain hazards even though several new developments

have been made in Earth remote sensing in recent years (Kirschbaum et al. 2019). Besides, the other factors involved in paraglacial rock-slope stability, such as lithology, intact rock strength, rock mass quality and joint characteristics, cannot be evaluated or investigated from satellite images. Therefore, the detecting, early warning and understanding the catastrophic geo-disasters in high-mountain region is still full of challenges.

Referring to speeding-up global change and regional warming in the high Himalaya, great risk of glacial geohazards accompanied by glacier shrinking (Guo et al. 2020) may be enhanced in the future. This situation might even be strengthened somewhat if earthquake activities enhanced, which is expected being one of the seismically active regions of the world, and engineering activity overlays inappropriately. Immediate attention to possible chain-like disasters in the high Himalaya, and collaborative satellite observations on geohazards-prone zones at multiple spatio-temporal scales, all are very necessary. Multi satellite observations together with automatic weather stations and dense seismological observations will be very helpful to investigate the geohazard risk and to understand the development process and final triggering.

Acknowledgment

The authors are grateful to the two anonymous referees and the Editor Professor Vincenzo Lapenna for their useful comments/suggestions that have helped us to improve earlier version of the manuscript.

Author contributions

Lixin Wu initiated this study, designed and developed the methods, and Wenfei Mao and Lixin Wu wrote the manuscript and revised it, and Ramesh discussed with Wu on this study, contributed some good ideas and improved the manuscript, and Yuan Qi calculated the MBT variations, and Busheng Xie reconstructed the 3D model of rockslide block, and Yingjia Liu calculated the ice cover variations, and Yifan Ding constructed the DEM model and processed the images from Sentinel-2, and Wenfei Mao and Zilong Zhou developed the conceptual mechanical model for rockslide block, and Jia Li analysed the background of glacial change in high Himalayan region.

Conflict of interest

The authors declare that they have no conflict of interest.

Availability of data and materials

The data that support the findings of this study are available from the first author.

Funding

This work was jointly supported by the Key Program of National Nature Science Foundation of China (41930108), the Basic Science Center by the National Natural Science Foundation of China (72088101), the Project funded by China Postdoctoral Science Foundation (2021M693550), and the Talents Gathering Program of Hunan Province, China (2018RS3013).

References

Ambrosi C, Strozzi T, Scapozza C, Wegmüller U. 2018. Landslide hazard assessment in the Himalayas (Nepal and Bhutan) based on Earth-Observation data. Eng Geol. 237:217–228.

Ballantyne CK. 2002. Paraglacial geomorphology. Quaternary Sci Rev. 21(18–19):1935–2017.

Barton N, Choubey V. 1977. The shear strength of rock joints in theory and practice. Rock Mech. 10(1–2):1–54.

Bessette-Kirton EK, Jeffrey AC. 2020. A 36-year record of rock avalanches in the Saint Elias Mountains of Alaska, with implications for future hazards.Frontiers in Earth Science. 8 (2020): 293.

Champati Ray PK, Chattoraj SL, Bisht MPS, Kannaujiya S, Pandey K, Goswami A. 2016. Kedarnath disaster 2013: causes and consequences using remote sensing inputs. Nat Hazards. 81(1):227–243.

Cook KL, Rekapalli R, Dietze M, Pilz M, Cesca S, Rao NP, Srinagesh D, Paul H, Metz M, Mandal P, et al. 2021. Detection and potential early warning of catastrophic flow events with regional seismic networks. Science. 374(6563):87–92.

Davies MCR, Hamza O, Harris C. 2001. The effect of rise in mean annual temperature on the stability of rock slopes containing ice-filled discontinuities. Permafrost Periglac Process. 12(1):137–144.

Fischer L, Huggel C, Kääb A, Haeberli W. 2013. Slope failures and erosion rates on a glacierized high-mountain face under climatic changes. Earth Surf Process Landforms. 38(8): 836–846.

Fish AM, Zaretsky YK. 1997. Ice strength as a function of hydrostatic pressure and temperature. CRREL Rep. 6–97.

Gautam R, et al. 2009. Enhanced pre-monsoon warming over the Himalayan-Gangetic region from 1979 to 2007. Geophys Res Lett. 36:L07704.

Glade T, Crozier MJ. 2005. The nature of landslide hazard impact. In: Glade T, Anderson MG, Crozier MJ (Eds.), Landslide Hazard and Risk. John Wiley & Sons Ltd., Chichester. pp: 43–74.

Gruber S, Haeberli W. 2007. Permafrost in steep bedrock slopes and its temperature related destabilization following climate change. J Geophys Res Earth. 112:F02S18.

Guo L, et al. 2020. The surge of the Hispar Glacier, Central Karakoram: SAR 3-D flow velocity time series and thickness changes. J Geophys Res. Sol Ea. 125:e2019JB018945.

Haeberli W. 1997. Slope stability problems related to glacier shrinkage and permafrost degradation in the Alps. Ecol Geol Helv. 90:407–414.

Hallet B. 1983. The breakdown of rock due to freezing: a theoretical model. Proceedings of the 4th International Conference. Natl. Acad. Press. p. 433–438.

Heim A, Gansser A. 1939. Central Himalaya, Geological observation of the Swiss Expedition in 1936. Mem Soc Helv Sci Nat. 73:1–245.

Jiang RC, et al. 2021. The Landslide Hazard Chain in the Tapovan of the Himalayas on 7 February 2021. Geophys Res Lett. e2021GL093723.

Kääb A, Leinss S, Gilbert A, Bühler Y, Gascoin S, Evans SG, Bartelt P, Berthier E, Brun F, Chao W-A, et al. 2018. Massive collapse of two glaciers in western Tibet in 2016 after surge-like instability. Nat. Geosci. 11(2):114–120.

Kemeny J. 2003. The time-dependent reduction of sliding cohesion due to rock bridges along discontinuities: a fracture mechanics approach. Rock Mech. Rock Eng. 36(1):27–38.

Kirschbaum D, Watson CS, Rounce DR, Shugar DH, Kargel JS, Haritashya UK, Amatya P, Shean D, Anderson ER, Jo M, et al. 2019. The state of remote sensing capabilities of cascading hazards over High Mountain Asia. Front Earth Sci. 7:197.

Kothyari GC, et al. 2021. Reconstruction of active surface deformation in the Rishi Ganga basin, Central Himalaya using PSInSAR: a feedback towards understanding the 7th February 2021 Flash Flood. Adv Space Res.

Krautblatter M, Funk D, Günzel FK. 2013. Why permafrost rocks become unstable: a rock-ice-mechanical model in time and space. Earth Surf Process Landforms. 38(8):876–887.

Leinss S, Bernardini E, Jacquemart M, Dokukin M. 2021. Glacier detachments and rock-ice avalanches in the Petra Pervogo range, Tajikistan (1973–2019). Nat Hazards Earth Syst Sci. 21(5):1409–1429.
McColl ST. 2012. Paraglacial rock-slope stability. Geomorphology. 153–154:1–16.
Meena SR, Bhuyan K, Chauhan A, Singh RP. 2021a. Changes in the flood plains and water quality along the Himalayan rivers after the chamoli disaster of 7 February 2021. Int J Remote Sens. 42(18):6984–7001.
Meena SR, Bhuyan K, Chauhan A, Singh RP. 2021b. Snow covered with dust after Chamoli rockslide: inference based on high-resolution satellite data. Remote Sens Lett. 12(7):704–714.
Meena SR, Chauhan A, Bhuyan K, Singh RP. 2021c. Chamoli disaster: pronounced changes in water quality and flood plains using Sentinel data. Environ Earth Sci. 80(17):601.
Negi HS, Kanda N, Shekhar MS, Ganju A. 2018. Recent wintertime climatic variability over the North West Himalayan cryosphere. Curr Sci. 114(04):760–770.
Nichols TC. 1980. Rebound, its nature and effect on engineering works. Q J Eng Geol Hydroge. 13(3):133–152.
Noetzli J, Gruber S, Kohl T, Salzmann N, Haeberli W. 2007. Three-dimensional distribution and evolution of permafrost temperatures in idealized high-mountain topography. J Geophys Res. 112(F2):F02S13.
Pandey P, Chauhan P, Bhatt CM, Thakur PK, Kannaujia S, Dhote PR, Roy A, Kumar S, Chopra S, Bhardwaj A, et al. 2021. Cause and process mechanism of rockslide triggered flood event in Rishiganga and Dhauliganga River Valleys, Chamoli, Uttarakhand, India using satellite remote sensing and in situ observations. J Indian Soc Remote Sens. 49(5):1011–1024.
Paterson WSB. 1994. Physics of Glaciers, Third Edition. Oxford, New York and Tokyo: Elsevier.
Planet Team 2018. Planet Application Program Interface: In Space for Life on Earth. San Francisco, CA. https://api.planet.com.
Qi Y, Wu L, Mao W, Ding Y, He M. 2021. Discriminating possible causes of microwave brightness temperature positive anomalies related with Wenchuan Earthquakes. IEEE Trans Geosci Remote Sensing. 59(3):1903–1966.
Rao NP, Rekapalli R, Srinagesh D, Tiwari VM, Hovius N, Cook KL, Dietze M. 2021. Seismological rockslide warnings in the Himalaya. Science. 372(6539):247.
Renoj JT, et al2021. Hanging glacier avalanche (Raunthigad-Rishiganga) and Debris flow disaster of 7th February 2021, Uttarakhand, India, A Preliminary assessment. Preprint at https://europepmc.org/article/ppr/ppr302068.
Ryzhkin IA, Petrenko VF. 1997. Physical mechanisms responsible for ice adhesion. J Phys Chem B. 101(32):6267–6270.
Sabin TP, et al. 2020. Assessment of climate change over the Indian region: a report of the ministry of earth sciences (MOES), government of India, Krishnan, R., Sanjay, J., Gnanaseelan, C., Mujumdar, M., Kulkarni, A., & Chakraborty, S. (eds). Springer, Singapore, p. 207–222.
Sahoo PK, Kumar S, Singh RP. 2000. Neotectonic studies of Ganga and Yamuna Tear Faults, NW Himalaya using remote sensing and GIS. Int J Remote Sens. 21(3):499–518.
Schneider D, Huggel C, Haeberli W, Kaitna R. 2011. Unraveling driving factors for large rock–ice avalanche mobility. Earth Surf Process Landforms. 36(14):1948–1966.
Shugar DH, Jacquemart M, Shean D, Bhushan S, Upadhyay K, Sattar A, Schwanghart W, McBride S, de Vries MVW, Mergili M, et al. 2021. A massive rock and ice avalanche caused the 2021 disaster at Chamoli, Indian Himalaya. Science. 373(6552):300–306.
Taber S. 1930. The mechanics of frost heaving. J Geol. 38(4):303–317.
Ulaby FT, Long DF. 2014. microwave radar and radiometric remote sensing. University of Michigan Press, United States of America.
Valdiya KS. 1980. Geology of the Kumaun Lesser Himalaya. Wadia Inst Himalayan Geol. 291
Valdiya KS, Goel OP. 1983. Lithological subdivision and petrology of the great Himalayan Vaikrita group in Kumaun, india. J Earth Syst Sci. 92(2):141–163.
Walder J, Hallet B. 1985. A theoretical model of the fracture of rock during freezing. Geol Soc Am Bull. 96(3):336–346.